

# Instability and disturbance amplification in a mixed-convection boundary layer

By ROBERT A. BREWSTER<sup>1</sup> AND BENJAMIN GEBHART<sup>2</sup>

<sup>1</sup>IBM Corporation, Hopewell Junction, NY 12533, USA

<sup>2</sup>Department of Mechanical Engineering and Applied Mechanics, University of Pennsylvania, Philadelphia, PA 19104-6315, USA

(Received 2 October 1990 and in revised form 8 January 1991)

The stability of a laminar mixed-convection boundary layer adjacent to a vertical isothermal surface is examined, using linear stability theory and the parallel-flow approximations. The analysis is valid when the imposed forced-convection effects are small compared to natural-convection effects. The stability equations are solved numerically for aiding and opposing forced-convection effects, for  $Pr = 0.733$  (air) and 6.7 (water). For aiding mixed convection in air, a new feature was found. A small, separated region of instability arises upstream of the ‘conventional’, or ‘primary’, neutral curve. In this region, selective amplification of a narrow band of disturbance frequencies occurred, but disturbance growth was small. Further downstream, disturbance growth rates in flows with an aiding free stream are slower than in natural convection. The opposite is true for an opposing free stream in air. Selective disturbance amplification occurred downstream for all conditions, as in natural convection. In water, an aiding flow was destabilizing compared to natural convection, and an opposing flow was stabilizing. Evidence of a separated upstream region of instability was also found for aiding mixed convection in water. However, converged solutions could not be obtained in this circumstance.

---

## 1. Introduction

Mixed-convection flows, which result from simultaneous buoyancy and forced flow effects, arise in environmental and technological processes ranging from atmospheric convection to electronics cooling. However, until recently, these flows have received relatively little attention. A thorough review of the work to date in this area is given by Gebhart *et al.* (1988). A notable feature of external laminar mixed-convection boundary-layer flows is that forced convection dominates the buoyancy effect near the leading edge of a developing flow. Natural convection dominates farther downstream.

However, a vigorous laminar flow eventually becomes unstable and turbulent downstream. Visualizations by Eckert & Soehngen (1951) indicated that the transition to turbulence in purely buoyancy-driven (natural convection) flows begins with the amplification of small disturbances in a laminar flow. Since the disturbances are small initially, linear stability theory has been widely used to predict the conditions of initial instability and subsequent downstream disturbance growth. Excellent agreement between linear stability theory and experimental data has been obtained (see Gebhart *et al.* 1988).

In general, only a narrow band of disturbance component frequencies is strongly

amplified in external natural-convection flows. This 'selective amplification' was first demonstrated by the calculations of Dring & Gebhart (1968). Experiment (Jaluria & Gebhart 1975) and theory (Audunson & Gebhart 1976) have shown that this selectivity persists downstream into the region where nonlinear effects and secondary mean flows develop. This behaviour differs from that of external forced-convection boundary layers, which amplify a wide band of disturbance component frequencies.

Although disturbance amplification in external natural-convection flows is fairly well understood, external mixed-convection flows have received relatively little attention. The earliest studies of mixed-convection instability examined flows adjacent to vertical (Mucoglu & Chen 1978), inclined (Chen & Moutsoglou 1979), and horizontal (Chen & Mucoglu 1979) isothermal flat surfaces. Since similarity does not arise for mixed-convection flow parallel to a flat surface, the undisturbed flow and temperature solutions were obtained using the local non-similarity method.

The local non-similarity method is an approximate method of solution of the boundary-layer equations for non-similar flows. The equations are first subjected to a coordinate transformation, and non-similar terms in the equations are defined as new variables. The transformed boundary-layer equations are then differentiated to provide differential equations for these new variables. Such a procedure of defining new variables and differentiating the transformed boundary-layer equations may continue indefinitely. However, at some level non-similar terms are omitted from the formulation, to close the system of equations. This measure makes the accuracy of the local non-similarity method difficult to assess.

The results of Mucoglu & Chen (1978), Chen & Moutsoglou (1979) and Chen & Mucoglu (1979) were limited to small values of a non-dimensional buoyancy parameter, which correspond to the forced-convection-dominated conditions near the leading edge of the plate. Neutral stability curves were given for  $Pr = 0.7$  and  $7.0$ , which are characteristic of air and water, respectively. In both cases, the flow along vertical or inclined surfaces was more stable when the forced flow was aided by the buoyancy effect. The stability of such flows decreased as the surface was inclined from the vertical. For flow over horizontal plates, however, flows with aiding buoyancy (buoyancy force directed away from the surface) were less stable than those with opposing buoyancy.

In these earlier studies, results were given in terms of a downstream  $x$ -dependent buoyancy parameter. This leads to some inconvenience in determining the location of neutral stability. This difficulty was overcome by Carey & Gebhart (1983) in an investigation of the stability of mixed-convection flow adjacent to a vertical surface dissipating a uniform heat flux. The undisturbed flow for large downstream distances was determined using matched asymptotic expansions (Carey & Gebhart 1982). All results are in terms of an  $x$ -independent parameter which is proportional to the free-stream velocity,  $u_\infty$ . In air, the mixed convection had a strong effect on both the stability and the disturbance-amplification characteristics. The effect of a forced flow was much weaker in water. Their measurements in air agreed well with the theoretical results.

Lee, Chen & Armaly (1987*a, b*, 1988) have studied the stability of aiding mixed convection adjacent to a vertical and inclined isothermal flat surface. The first study considers flows with small forced-convection effects, while the second two encompass the entire mixed-convection regime. The disturbance equations used in all of these studies include some of the effects of the non-parallelism of the base flow. However, any attempt to include non-parallel flow effects must be done in a consistent manner.

As shown by Wakitani (1985), for example, some higher-order boundary-layer terms appear in conjunction with the first-order corrections for non-parallel flow effects. These higher-order terms were not included by Lee *et al.* Also, only neutral stability curves were given. The downstream growth characteristics of disturbances were not determined.

The present study concerns the stability of a mixed-convection flow far from the leading edge of an isothermal, vertical flat surface. This is a buoyancy-driven flow subject to a relatively small forced flow effect. Perturbation expansions are used to determine the undisturbed flow. A consistent linear stability theory is then used to obtain both neutral stability and constant disturbance-amplification contours, for  $Pr = 0.733$  (air) and  $Pr = 6.7$  (water). Results are presented for both aiding and opposing mixed-convection flows.

## 2. Undisturbed flow solutions

The undisturbed laminar mixed-convection flow is first determined for use in the disturbance analysis. This flow is adjacent to a flat vertical surface at uniform and constant temperature  $t_0$  (see figure 1). A vertical forced flow with uniform free-stream velocity,  $u_\infty$ , and free-stream temperature,  $t_\infty$ , is present. All fluid properties are assumed constant, except for the density. Then, the Boussinesq approximations are made.

The solutions for conditions far from the leading edge of the plate are desired. Perturbation techniques have been used by Eshghy (1964), Szewczyk (1964) and Merkin (1969) to study this flow. Merkin noted the omission of necessary logarithmic terms in the second-order expansions of the earlier investigators. The resulting analysis is outlined below, with some changes in the definitions of dimensionless parameters.

A dimensionless stream function,  $f(x, \eta)$ , and dimensionless temperature,  $\theta(x, \eta)$ , are defined in terms of the usual stream function,  $\psi(x, y)$ , and difference between the local and ambient fluid temperatures,  $t(x, y) - t_\infty$ :

$$f(x, \eta) = \frac{\psi(x, y)}{\nu G(x)}, \quad (2.1)$$

$$\theta(x, \eta) = \frac{t(x, y) - t_\infty}{t_0 - t_\infty}, \quad (2.2)$$

where 
$$\eta = \frac{yG(x)}{4x} \quad (2.3)$$

and 
$$G(x) = 4 \left( \frac{Gr_x}{4} \right)^{\frac{1}{4}}; \quad Gr_x = \frac{g\beta_t(t_0 - t_\infty)x^3}{\nu^2}. \quad (2.4)$$

The coordinate  $x$  is measured vertically from the leading edge of the surface, and  $y$  is the coordinate normal to the surface (see figure 1). The fluid properties  $\nu$  and  $\beta_t$  are the kinematic viscosity and thermal expansion coefficient, respectively. The acceleration due to gravity is  $g$ .

The mixed-convection flow under consideration does not admit similarity solutions. However, far from the leading edge of the surface, the buoyancy effect becomes relatively much larger than the forced-convection effect. Therefore, a

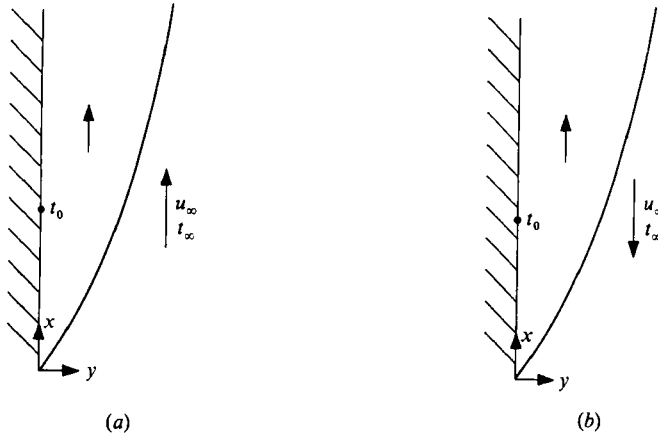


FIGURE 1. Schematic representation of mixed-convection flow adjacent to a vertical isothermal surface: (a) aiding mixed convection; (b) opposing mixed convection. The buoyancy force is directed upward in each case.

natural-convection flow is perturbed to include a small free-stream velocity. The perturbation expansions are

$$f(x, \eta) = f_0(\eta) + \epsilon(x)f_1(\eta) + \dots, \quad (2.5)$$

$$\theta(x, \eta) = \theta_0(\eta) + \epsilon(x)\theta_1(\eta) + \dots, \quad (2.6)$$

where  $f_0(\eta)$  and  $\theta_0(\eta)$  are a natural-convection flow in a quiescent ambient medium, and the perturbation parameter  $\epsilon(x)$  is defined as

$$\epsilon(x) = 4 \frac{Re_x}{G^2(x)}, \quad (2.7)$$

$$Re_x = \frac{u_\infty x}{\nu}, \quad (2.8)$$

with  $G(x)$  defined by (2.4).

It is convenient to present results in terms of an  $x$ -independent parameter  $\bar{R}$  which is proportional to the vigour of the forced flow. This is achieved by dividing  $Re_x$  by the power of  $Gr_x$ , which eliminates the  $x$ -dependence. The result is

$$\bar{R} = \frac{Re_x}{Gr_x^{\frac{1}{2}}} = u_\infty \left( \frac{1}{g\beta_t \nu (t_0 - t_\infty)} \right)^{\frac{1}{2}}, \quad (2.9)$$

where we take the real root in (2.9). When  $\bar{R}$  is positive  $u_\infty$  and the buoyancy force are in the same direction. This is called an aiding mixed-convection flow. An opposing mixed-convection flow arises when  $u_\infty$  and the buoyancy force are in opposite directions ( $\bar{R} < 0$ ). Natural convection occurs when  $u_\infty = 0$  ( $\bar{R} = 0$ ). Examples of aiding and opposing mixed-convection flows with upwardly directed buoyancy forces are shown in figures 1(a) and 1(b), respectively.

Using (2.4) and (2.9) with (2.7) yields

$$\epsilon(x) = \bar{R}/G^{\frac{1}{2}}. \quad (2.10)$$

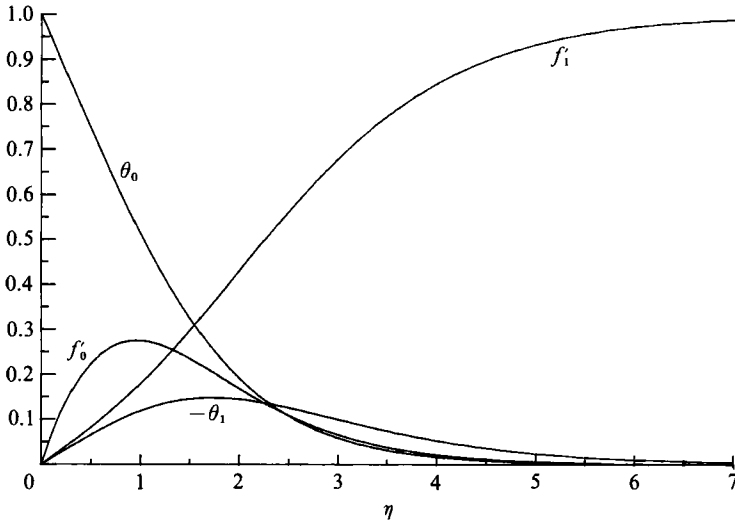


FIGURE 2. Undisturbed flow solutions for  $Pr = 0.733$  (air).

From this point onward only the first two terms in the expansions (2.5) and (2.6) are considered. This is consistent with the boundary-layer and parallel-flow approximations which will be made in deriving the disturbance equations.

The expansions (2.5) and (2.6) are substituted into the boundary-layer equations. Using the Boussinesq approximations and neglecting viscous dissipation and pressure work in the energy equation, the governing equations for  $f_0, f_1, \theta_0,$  and  $\theta_1$  are

$$f_0''' + 3f_0 f_0'' - 2f_0'^2 + \theta_0 = 0, \tag{2.11 a}$$

$$\theta_0'' + 3Pr f_0 \theta_0' = 0, \tag{2.11 b}$$

$$f_1''' + 3f_0 f_1'' + f_0'' f_1 - 2f_0' f_1' + \theta_1 = 0, \tag{2.12 a}$$

$$\theta_1'' + Pr [2f_0' \theta_1 + f_1 \theta_0' + 3f_0 \theta_1'] = 0, \tag{2.12 b}$$

where  $Pr$  is the Prandtl number:

$$Pr = \frac{\nu}{\alpha_t}, \tag{2.13}$$

and where  $\alpha_t$  is the thermal diffusivity of the fluid. The associated boundary conditions are

$$f_0(0) = f_0'(0) = \theta_0(0) - 1 = f_0'(\infty) = \theta_0(\infty) = 0, \tag{2.14 a}$$

$$f_1(0) = f_1'(0) = \theta_1(0) = f_1'(\infty) - 1 = \theta_1(\infty) = 0. \tag{2.14 b}$$

The system (2.11), (2.12), (2.14) was solved numerically using a fourth-order predictor-corrector method with a shooting technique. The boundary conditions at infinity were replaced with asymptotic solutions to (2.11) and (2.12), valid as  $\eta \rightarrow \infty$  (Brewster 1988). These were used as starting values at some large  $\eta = \eta_{\text{edge}}$ . The integration proceeded inward from  $\eta_{\text{edge}}$  toward the surface at  $\eta = 0$ .

Numerical solutions for the functions  $f_0', \theta_0, f_1'$  and  $\theta_1$  are plotted in figures 2 and 3 for  $Pr = 0.733$  and 6.7, respectively. The functions  $f_0'$  and  $\theta_0$  are the natural-convection components, and  $f_1'$  and  $\theta_1$  are the first-order corrections for forced-convection effects. The functions  $f_1'$  and  $\theta_1$  have not previously appeared in the literature for  $Pr = 6.7$ .

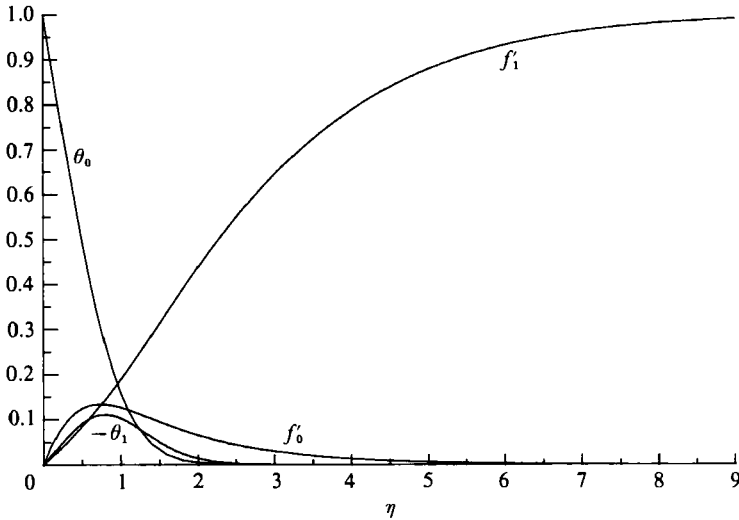


FIGURE 3. Undisturbed flow solutions for  $Pr = 6.7$  (water).

### 3. Disturbance equations

Linear stability theory is used to derive equations governing the behaviour of small disturbances which arise in the mixed-convection flow. The velocity components, temperature and pressure are each expressed as the sum of a mean and a disturbance component:

$$u = \bar{u} + u', \quad v = \bar{v} + v', \quad t = \bar{t} + t', \quad p = \bar{p} + p'. \quad (3.1a-d)$$

The stream function and temperature disturbance components are taken to be of the form

$$\psi'(x, y, \tau) = \nu G \phi(\eta) \exp [i(\hat{\alpha}x - \hat{\beta}\tau)], \quad (3.2a)$$

$$t'(x, y, \tau) = (t_0 - t_\infty) s(\eta) \exp [i(\hat{\alpha}x - \hat{\beta}\tau)], \quad (3.2b)$$

where

$$u' = \frac{\partial \psi'}{\partial y}; \quad v' = -\frac{\partial \psi'}{\partial x}. \quad (3.3)$$

Here,  $\hat{\alpha}$  is taken as complex and  $\hat{\beta}$  as real. Physically, the real part of  $\hat{\alpha}$  is then the disturbance wavenumber. The imaginary part is the downstream amplification rate. The disturbance frequency is  $\hat{\beta}$ . Both  $\phi(\eta)$  and  $s(\eta)$  are, in general, complex functions of the real variable  $\eta$ .

To obtain the disturbance equations, (3.1) are substituted into the two-dimensional Navier–Stokes equations, with the Boussinesq approximations. After subtracting the boundary-layer equations in the mean quantities, all nonlinear terms in the disturbance quantities are omitted. The parallel-flow approximations are then employed. These amount to neglecting several small  $x$ -dependences, as discussed in detail by Hieber & Gebhart (1971).

Gaster (1974) has used a linear stability theory which accounts for non-parallelism in the base flow to study the instability of the Blasius flow. Wakitani (1985), following the method of Gaster, has examined non-parallel-flow effects on the instability of line-source plumes. The parallel-flow approximations are the first approximation in a more extensive theory which includes non-parallel-flow effects. For the Blasius flow and the line-source plume, the first corrections to the eigenfunctions and amplification rate are  $O(Re_x^{-1/2})$  and  $O(G^{-1})$ , respectively. The

smallest value of  $G$  for which instability was found for any of the conditions considered in this study was 17.32. Therefore, non-parallel-flow effects would, at most, amount to approximately a 6% correction.

After the above approximations are made, the momentum equations are combined to eliminate the disturbance pressure. Then, (3.2) and (3.3) are substituted into the vorticity and energy equations. The resulting disturbance-amplitude equations, sometimes called the Orr-Sommerfeld equations, are

$$\left(f' - \frac{\beta}{\alpha}\right)(\phi'' - \alpha^2\phi) - f''' \phi = \frac{1}{i\alpha G} \{\phi^{iv} - 2\alpha^2\phi'' + \alpha^4\phi + s'\}, \quad (3.4a)$$

$$\left(f' - \frac{\beta}{\alpha}\right)s - \theta' \phi = \frac{1}{i\alpha G Pr} \{s'' - \alpha^2 s\}, \quad (3.4b)$$

where  $\alpha$  and  $\beta$  are dimensionless quantities defined as

$$\alpha = \frac{4x}{G} \hat{\alpha} = \alpha_r + i\alpha_i, \quad \beta = \frac{16x^2}{\nu G^3} \hat{\beta} \quad (3.5a, b)$$

The primes on  $f(x, \eta)$  and  $\theta(x, \eta)$  in (3.4) denote partial differentiation with respect to  $\eta$ , while the primes on  $\phi(\eta)$  and  $s(\eta)$  denote ordinary differentiation with respect to  $\eta$ .

As first discussed by Knowles & Gebhart (1968), thermal disturbances are damped out at a surface of relatively large thermal capacity, so  $s(0) = 0$ . This is assumed here. The complete set of disturbance boundary conditions is then

$$\phi(0) = \phi'(0) = s(0) = \phi(\infty) = \phi'(\infty) = s(\infty) = 0. \quad (3.6)$$

The eigensystem defined by (3.4) and (3.6) is sixth order, coupled, and linear in the eigenfunctions  $\phi(\eta)$  and  $s(\eta)$ . The eigenvalues are any two of  $\alpha_r$ ,  $\alpha_i$ ,  $\beta$  or  $G$ . The remaining two are specified. The eigenvalues and eigenfunctions are then determined by numerical integration. This procedure is discussed in the following section.

#### 4. Numerical integration procedure

As noted by Hieber & Gebhart (1971), the eigenfunctions  $\phi(\eta)$  and  $s(\eta)$  may be expressed in terms of six pairs of linearly independent solutions. Three pairs may be shown to be exponentially large as  $\eta \rightarrow \infty$ . These solutions cannot satisfy the boundary conditions (3.6) at the outer edge of the disturbance boundary region. Therefore, each eigenfunction is written in terms of the remaining three pairs of solutions:

$$\phi(\eta) = B_1 \phi_1(\eta) + B_2 \phi_2(\eta) + B_3 \phi_3(\eta), \quad (4.1a)$$

$$s(\eta) = B_1 s_1(\eta) + B_2 s_2(\eta) + B_3 s_3(\eta), \quad (4.1b)$$

where  $B_1, B_2$  and  $B_3$  are complex constants. The constant  $B_1$  may be chosen as unity. This scales the disturbance magnitude arbitrarily.

Points on the neutral stability curve ( $\alpha_i = 0$ ) are to be found first. Values for  $Pr, \bar{R}$  and  $G$  are chosen, and guesses are then made for the eigenvalues  $\alpha_r$  and  $\beta$ . The solution scheme consists of integrating the disturbance equations separately for each of the three pairs of linearly independent solutions. All integrations were accomplished using a fourth-order predictor-corrector method.

Each integration began at the outer edge of the disturbance boundary region, using asymptotic solutions to the disturbance equations (3.4) there to replace the

boundary conditions at infinity (Brewster 1988). Each integration proceeded inward, from a large  $\eta = \eta_{\text{edge}}$ , to the surface (at  $\eta = 0$ ). When integration for each of the three pairs of linearly independent solutions was complete, two of the disturbance boundary conditions at  $\eta = 0$  were used to compute the complex constants  $B_2$  and  $B_3$ . The third boundary condition at  $\eta = 0$  was satisfied only if the guessed values for  $\alpha_r$  and  $\beta$  were correct. A Newton-Raphson technique was used to provide improved values of  $\alpha_r$  and  $\beta$ . Iteration continued in this way until the third boundary condition at  $\eta = 0$  was satisfied, to within some specified accuracy (typically  $10^{-4}$ ). Each application of this procedure yields one point on the neutral stability curve, for the specified values of  $Pr$  and  $\bar{R}$ .

The downstream disturbance growth characteristics were then determined. This growth is expressed as the ratio of the magnitude of a disturbance frequency component, at a downstream location,  $x = L$ , to its magnitude at the upstream location of neutral stability,  $x = x_N$ . The disturbance magnitude at an arbitrary  $x$  location is given by

$$A_x = \nu G \phi(\eta) \exp(-\hat{\alpha}_1 x). \quad (4.2)$$

Consistent with the parallel-flow approximations, the algebraic  $x$ -dependence of  $G$  and  $\phi$  may be neglected, compared to the exponential  $x$ -dependence. Then

$$\frac{dA_x}{A_x} = -\hat{\alpha}_1 dx \quad (4.3)$$

and integration at constant disturbance frequency,  $\beta$ , from  $x_N$  to a downstream location  $x = L$  yields

$$\frac{A_L}{A_N} = \exp\left[-\int_{x_N}^L \hat{\alpha}_1 dx\right] = e^A, \quad (4.4)$$

where  $A$  is the disturbance amplification parameter. Using (2.4) and (3.5a),  $A$  may be expressed as

$$A = -\frac{1}{3} \int_{G_N}^{G_L} \alpha_1 dG, \quad (4.5)$$

where  $G_N = G(x_N)$  and  $G_L = G(L)$ . The integration in (4.5) is carried out at constant  $B$ , defined as

$$B = \beta G^{\frac{1}{3}} = \frac{2\pi f \hat{g}}{\nu} \left[ \frac{g}{\nu^2} \beta_t (t_0 - t_\infty) \right]^{-\frac{2}{3}}. \quad (4.6)$$

Note that the  $x$ -independent dimensionless frequency,  $B$ , is proportional to the physical frequency,  $f$ .

From (4.4) and (4.5), the  $A = 0$  contour is the neutral ( $\alpha_1 = 0$ ) curve. Contours of constant  $A$ , at selected values greater than zero, were computed numerically. The simple trapezoidal rule was used to numerically evaluate the integral in (4.5). The resulting contours of constant  $A$  indicate the growth of a particular disturbance component as it is convected downstream, past the neutral curve, into the region of instability.

## 5. Results

In this section, results are given in the form of constant- $A$  contours and eigenfunctions, for aiding and opposing mixed-convection flows, in air and in water. These results are interpreted by comparing them with each other, and with results for natural-convection flows.

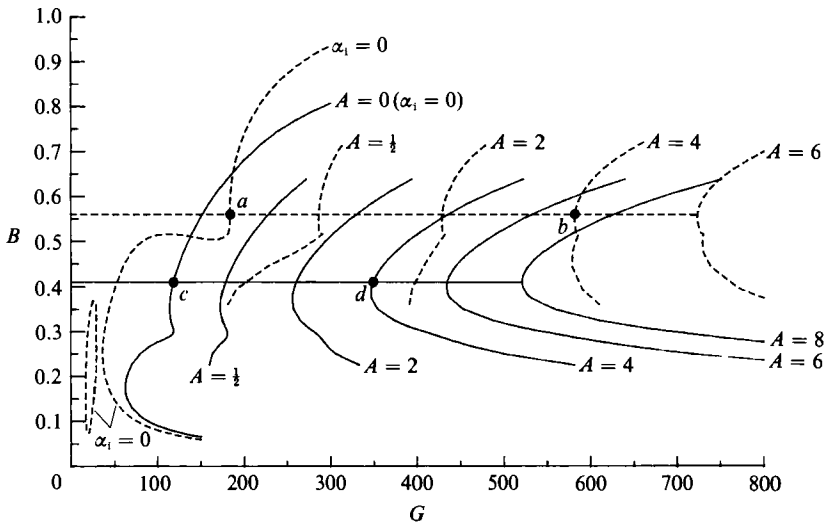


FIGURE 4. Amplification contours for aiding mixed convection (---,  $\bar{R} = 4$ ) and natural convection (—,  $\bar{R} = 0$ ) in air ( $Pr = 0.733$ ). The horizontal lines are the most amplified frequencies downstream.

5.1. Aiding mixed convection in air

Figure 4 compares constant- $A$  contours for natural convection,  $\bar{R} = 0$ , and for aiding mixed convection,  $\bar{R} = 4$ , in air ( $Pr = 0.733$ ) as the solid and dashed curves, respectively. Recall that  $\alpha_1 = 0$  (or  $A = 0$ ) represents neutral stability. These results are also characteristic of many other common gases. For example, the range  $0.6 \leq Pr \leq 0.8$  includes helium, hydrogen, oxygen, nitrogen and carbon dioxide. The value of  $\bar{R}$  for  $Pr = 0.733$  is limited to 4 to ensure that  $u_\infty$  is less than the local maximum natural convection velocity which would arise in the absence of forced flow.

As discussed in the introduction, natural-convection flows selectively amplify a very narrow band of disturbance component frequencies downstream. This effect also arises in mixed convection. The solid and dashed horizontal lines on figure 4 are the disturbance component frequencies, in terms of  $B$ , which are the most highly amplified as they are convected downstream, for natural and aiding mixed convection, respectively. These are chosen on the basis of a downstream location where  $A = 8$  (not shown for  $\bar{R} = 4$ ). The most amplified disturbance frequency far downstream, for aiding mixed convection, is seen to be  $B = 0.56$ , compared to  $B = 0.41$  for natural convection. Similar qualitative behaviour was seen by Carey & Gebhart (1983) for a uniform-heat-flux surface condition.

A very unexpected result of these calculations was that two neutral curves were found for aiding mixed convection in air. The expected, or ‘primary’, neutral curve for  $\bar{R} = 4$  lies at larger  $G$ . However, there is also a secondary, oval-shaped neutral curve upstream of this. This secondary region of instability is a very unusual feature, although a similar contour was seen by Lee *et al.* (1987*b*) for this flow.

Enlargements of this oval region of instability are shown in figure 5, in terms of both  $\alpha_1$  and  $A$ . The gaps near the top and bottom of the ovals are regions where converged eigenvalues and eigenfunctions could not be obtained. The contours on the far right-hand sides of figures 5(a) and 5(b) are the ‘nose’ of the primary neutral curve, shown as a dashed curve in figure 4. In figure 5(a), the contours of downstream

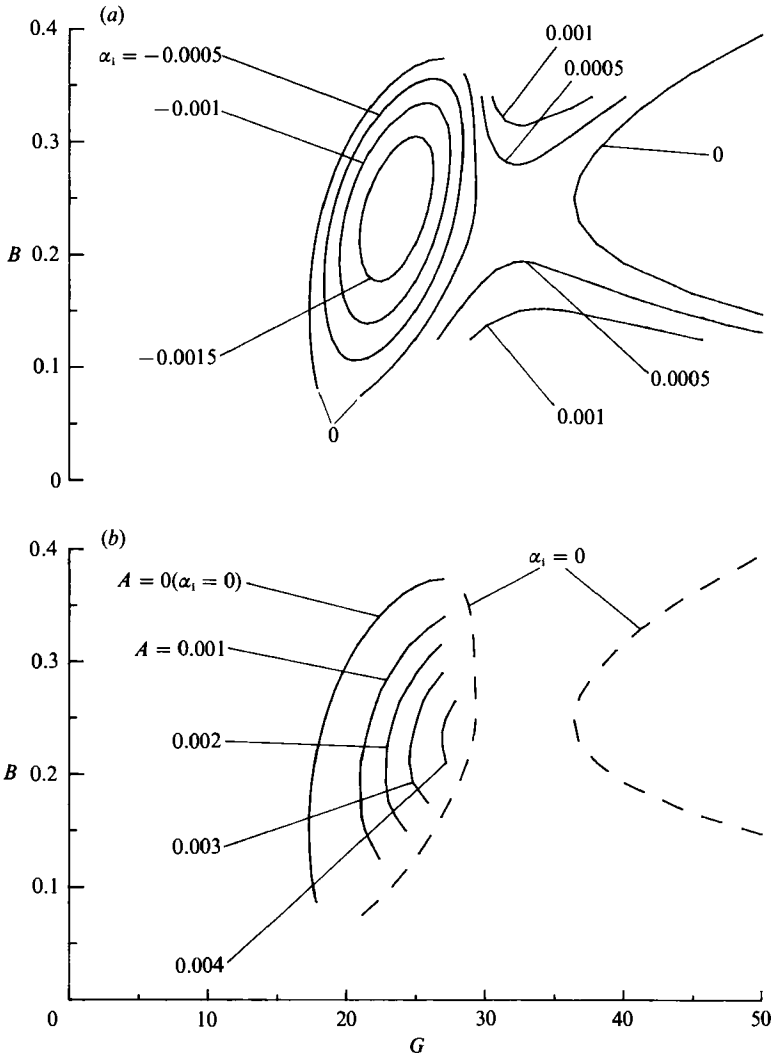


FIGURE 5. Enlargement of oval neutral region for aiding mixed convection ( $\bar{R} = 4$ ) in air ( $Pr = 0.733$ ), showing: (a) contours of constant  $\alpha_1$ ; (b) contours of constant  $A$ .

amplification rate,  $\alpha_1$ , have an oval shape. Outside and to the right of the oval neutral curve ( $\alpha_1 = 0$ ), several contours of  $\alpha_1 > 0$  are also shown. Since  $\alpha_1 > 0$ , the disturbances there are damped until they reach the primary neutral curve downstream.

Apparently, this oval region of instability disappears when the forced flow becomes large compared to the buoyancy-induced flow. Mucoglu & Chen (1978) have considered mixed convection with weak buoyancy effects and did not observe this feature. The vast literature on the instability of the Blasius flow also indicates that the oval unstable region is not present when there is no buoyancy.

The  $A$  contours in figures 4 and 5(b) are computed by integrating (4.5) from the value of  $G$  at which instability first occurs. For disturbance component frequencies corresponding to  $B < 0.37$ , instability first occurs on the oval neutral ( $\alpha_1 = 0$ ) curve, while for  $B > 0.37$ , instability first arises on the primary neutral ( $\alpha_1 = 0$ ) curve.

However, the computations revealed that  $A \approx 0$  on the primary neutral curve even for  $B < 0.37$ . That is, amplification inside the oval region, and subsequent damping just upstream of the primary neutral curve results in almost no contribution in the calculation of the  $A$  contours.

The constant- $A$  contours in the oval region indicate a maximum value of about  $A = 0.0043$ . That is, the disturbance amplitudes increase only by a factor of about 1.0043 over this separated region of instability. The  $A$  contours show the selective amplification of the frequency  $B \approx 0.24$  in this region. This frequency is, perhaps not surprisingly, the same as at the nose of the primary neutral curve.

Figure 6 shows the magnitudes of eigenfunctions, normalized by their respective maxima, for a point on the oval neutral curve of figure 5(b). These eigenfunctions are approximately one order of magnitude smaller than those found on the primary neutral curve, although both were scaled to unity by setting  $B_1 = 1$  in (4.1).

Downstream of the primary neutral curve, more rapid amplification occurs, as seen from the constant- $A$  contours of figure 4. This figure also shows that the aiding forced flow effect is destabilizing just downstream of the neutral stability curve. However, further downstream, the spatial amplification rate for mixed convection is much smaller. Near  $G \approx 150$ , the most amplified disturbances of the natural- and mixed-convection flows have about the same magnitude. Further downstream, disturbances in the mixed-convection flow grow less rapidly downstream.

#### *Explanation of slower downstream amplification*

Krishnamurthy & Gebhart (1989) have proposed an explanation for this effect, for aiding mixed-convection flows in air. The acceleration formula of Lin (1945) was used. This strictly applies only to the parallel flow of an inviscid fluid with a transverse velocity gradient. Assuming that the velocity gradient is in the  $y$ -direction, Lin showed that if a fluid element has an excess or defect of vorticity over the base flow, then it is subjected to an acceleration,  $a$ , in the  $y$ -direction, given by

$$a = \frac{\iint \{v'(x, y)\}^2 d\bar{\zeta}/dy dx dy}{\iint \zeta'(\xi, \chi) d\xi d\chi}, \quad (5.1)$$

where  $v'$  is a velocity component in the  $y$ -direction due to the vorticity excess or defect,  $\bar{\zeta}(y)$  is the vorticity distribution in the undisturbed flow, and  $\zeta'$  is the vorticity excess or defect. Therefore, the direction in which the fluid element is accelerated depends upon the signs of  $d\bar{\zeta}/dy$  and  $\zeta'$ .

A disturbance in the fluid motion may be regarded as the cross-stream exchange of two fluid elements with different vorticities. If there is a point of inflexion in the velocity profile (that is, if  $d\bar{\zeta}/dy = 0$  at some point in the vorticity field), then the exchanged fluid elements may each be accelerated away from their layers of origin. This is because  $\zeta'$  will have a different sign for the two fluid elements, and  $d\bar{\zeta}/dy$  changes sign across the inflexion point. Physically, counter-rotating vortices may arise which accelerate the fluid elements away from their original locations. The fluid motion is not stable under these circumstances.

The undisturbed flow vorticity gradients, for aiding, opposing and natural convection in air, are plotted as a function of  $\eta$  in figure 7. It is seen that the magnitude of the vorticity gradient near  $d\bar{\zeta}/dy = 0$  is smaller for aiding mixed convection than for natural convection. This led Krishnamurthy & Gebhart (1989) to

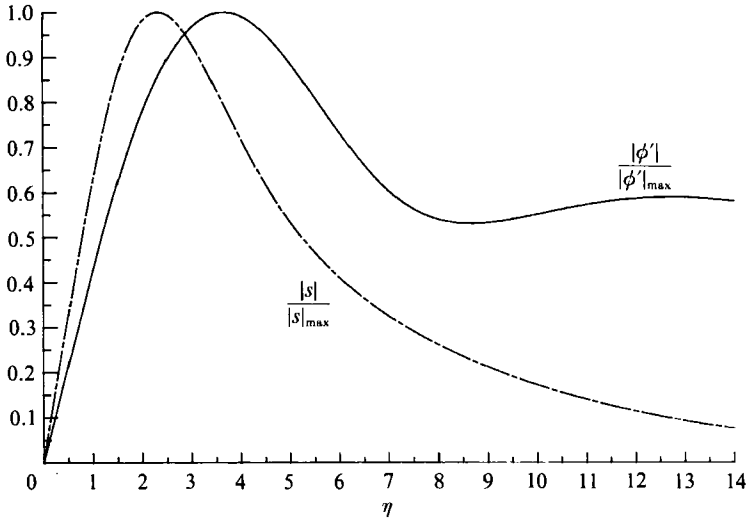


FIGURE 6. Magnitudes of the eigenfunctions for aiding mixed convection ( $\bar{R} = 4$ ) in air ( $Pr = 0.733$ ), normalized by their respective maxima, for the point ( $G = 17.94$ ,  $B = 0.225$ ) on the neutral curve of figure 5(b).

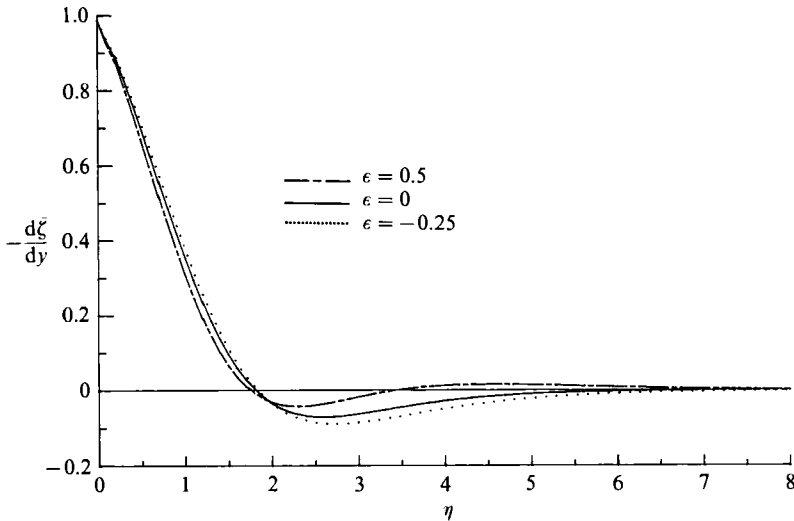


FIGURE 7. Vorticity fields for aiding mixed convection ( $\epsilon = 0.5$ ), opposing mixed convection ( $\epsilon = -0.25$ ), and natural convection ( $\epsilon = 0$ ) in air ( $Pr = 0.733$ ).

conclude that there is less tendency for fluid elements to move away from their layers of origin. Then, aiding mixed-convection flow is more 'stable' than natural convection. This explains the slower downstream amplification of the mixed-convection flow. However, the theory is inconsistent with the initial instability at lower  $G$ .

### 5.2. Opposing mixed convection in air

Constant-amplification contours for opposing mixed convection in air ( $\bar{R} = -2$ ,  $Pr = 0.733$ ) are shown in figure 8 by the dashed lines. Natural convection is again shown for comparison as solid curves. For opposing mixed-convection flows, it is

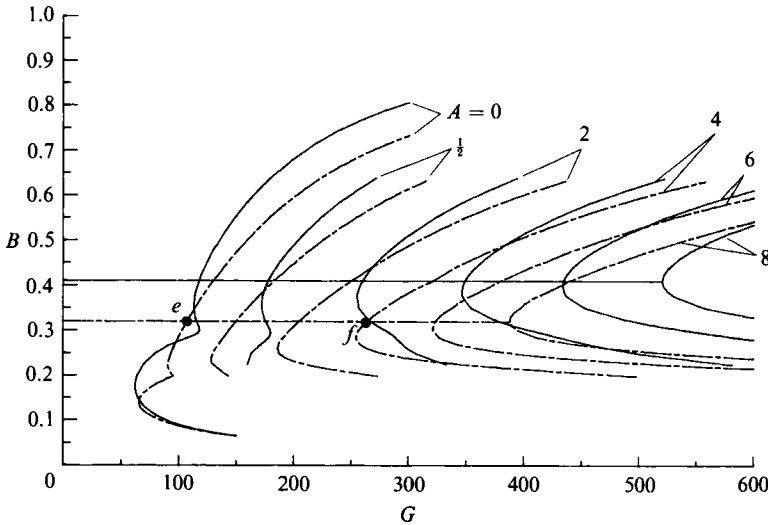


FIGURE 8. Amplification contours for opposing mixed convection (---,  $\bar{R} = -2$ ) and natural convection (—,  $\bar{R} = 0$ ) in air ( $Pr = 0.733$ ). The horizontal lines are the most amplified frequencies downstream.

necessary to avoid conditions for which boundary-layer separation occurs, since the analysis is then inappropriate. For air with  $\bar{R} = -2$ , separation does not occur over the range of  $G$  considered here.

Flows with an opposing effect are seen in figure 8 to be initially more stable than natural convection. However, downstream disturbance amplification is much faster. This faster downstream amplification is also consistent with (5.1). Figure 7 shows that the vorticity gradients of opposing mixed-convection flows near  $d\xi/dy = 0$  are larger than for a natural-convection flow. Therefore, according to (5.1), the acceleration of fluid elements away from their original locations will be greater in opposing mixed-convection flows than in natural-convection flows.

The most amplified frequency component for opposing mixed-convection flow, to  $A = 8$ , is  $B = 0.32$ , as shown by the horizontal dashed line on figure 8. This is at a lower frequency than the most amplified component for natural convection,  $B = 0.41$ , shown as a solid horizontal line.

#### *Disturbance-amplitude functions*

The magnitudes of typical eigenfunctions for aiding, opposing, and natural convection in air are shown in figure 9, normalized by their respective maxima. Each plot contains two pairs of eigenfunctions. One is for the point on the neutral curve corresponding to the most amplified frequency component downstream to  $A = 8$ . The second pair is for the same frequency on the  $A = 4$  contour. The locations on the stability planes for which the eigenfunctions are shown are represented by points (a-f) on figures 4 and 8.

The eigenfunction distributions across the disturbance boundary region are seen to be generally preserved as they are convected downstream. The downstream growth of  $\phi(\eta)$  accounts for only about 4% of the total downstream growth of  $\psi'$ . This is consistent with the parallel-flow approximations. The maxima of the eigenfunctions occur near the point of inflexion of the velocity profile,  $\eta \approx 1.8$ . This further emphasizes the importance of inflexion points in these instability mechanisms.

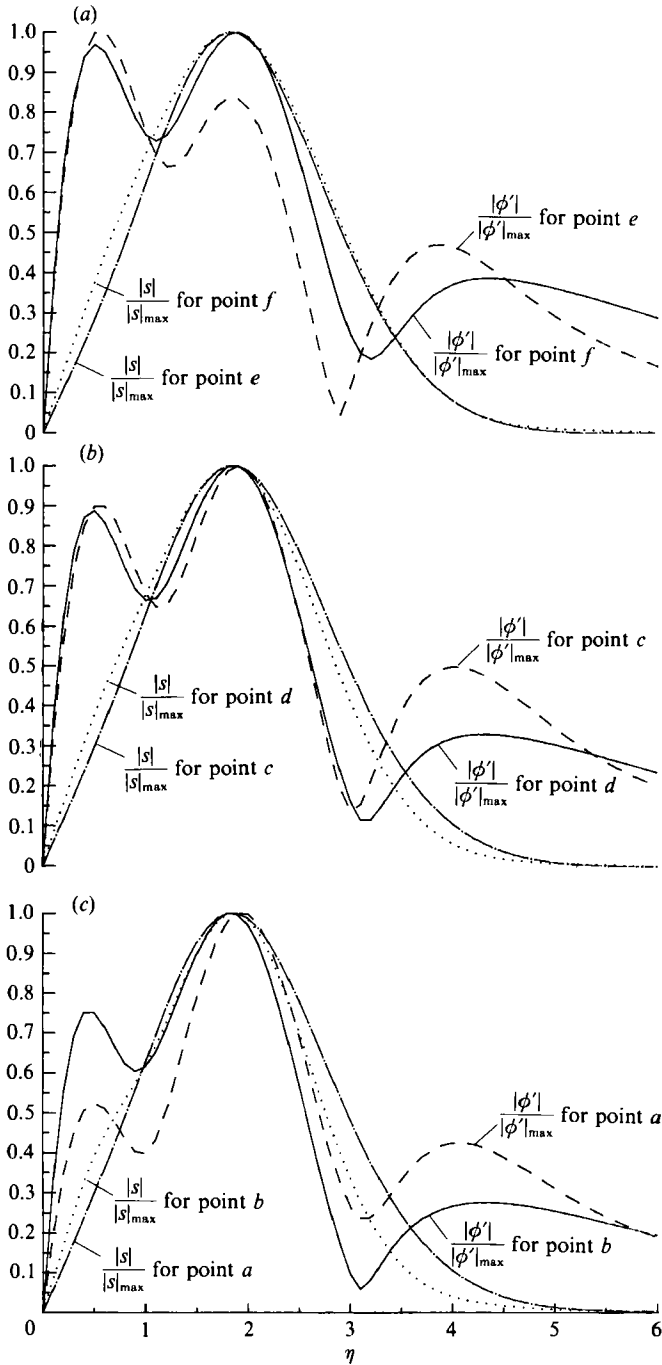


FIGURE 9. Magnitudes of the eigenfunctions in air ( $Pr = 0.733$ ), normalized by their respective maxima, for: (a) opposing mixed convection ( $\bar{R} = -2$ ), at points  $e$  and  $f$  on figure 8; (b) natural convection ( $\bar{R} = 0$ ), at points  $c$  and  $d$  on figure 4; (c) aiding mixed convection ( $\bar{R} = 4$ ), at points  $a$  and  $b$  on figure 4.

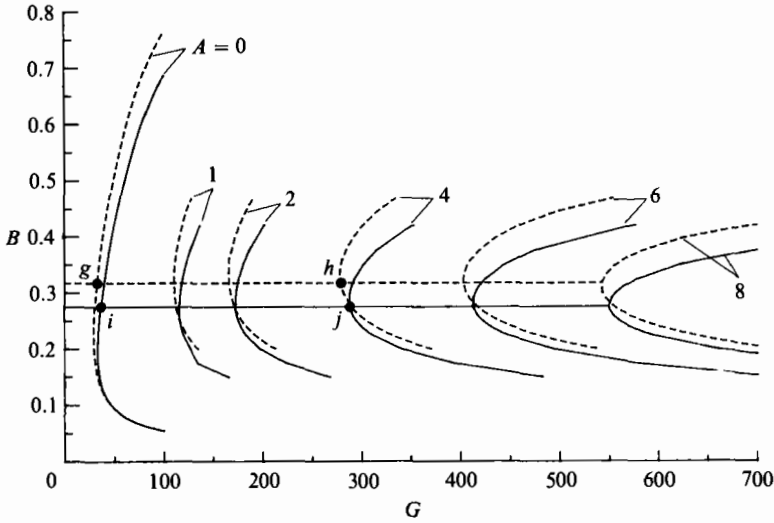


FIGURE 10. Amplification contours for aiding mixed convection (---,  $\bar{R} = 1$ ) and natural convection (—,  $\bar{R} = 0$ ) in water ( $Pr = 6.7$ ). The horizontal lines are the most amplified frequencies downstream.

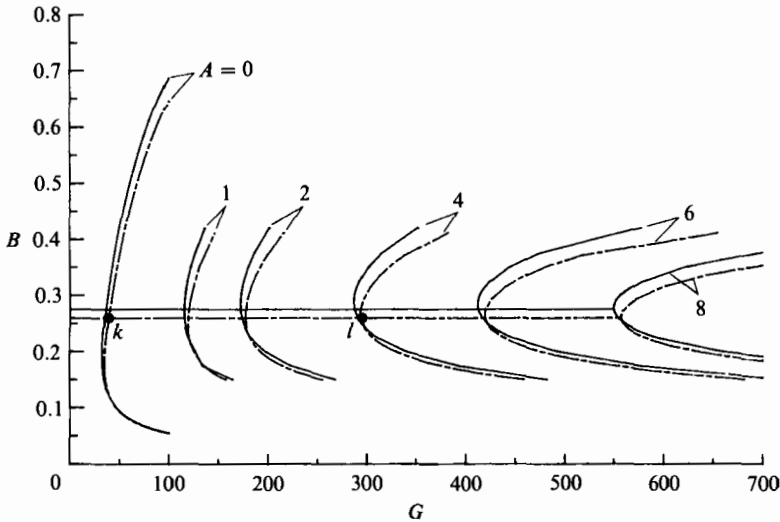


FIGURE 11. Amplification contours for opposing mixed convection (---,  $\bar{R} = -0.5$ ) and natural convection (—,  $\bar{R} = 0$ ) in water ( $Pr = 6.7$ ). The horizontal lines are the most amplified frequencies downstream.

*5.3. Aiding mixed convection in water*

The amplification plane for aiding mixed convection in water ( $\bar{R} = 1$ ,  $Pr = 6.7$ ) is shown in figure 10, as dashed lines. Comparable natural-convection contours for water ( $\bar{R} = 0$ ,  $Pr = 6.7$ ) are shown as solid lines. Other liquids which have Prandtl numbers near 6.7 are methanol at 30 °C and saturated Freon 11 near -50 °C.

The most amplified frequency component to  $A = 8$  is  $B = 0.32$ . This is higher than  $B = 0.28$  for natural convection. The same qualitative behaviour was seen for air. However, the forced flow effects are much smaller in water. Aiding mixed convection is slightly less stable than natural convection. The acceleration equation (5.1) does not explain this difference. This implies that buoyancy plays an important role not

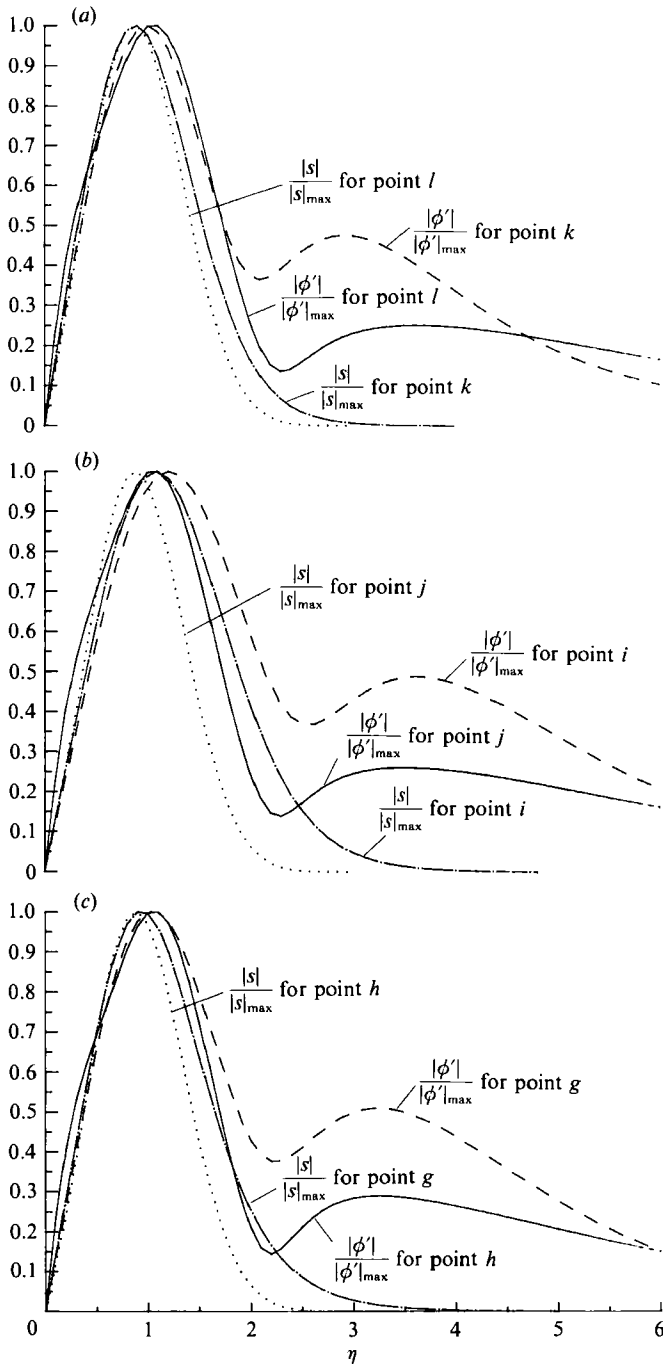


FIGURE 12. Magnitudes of the eigenfunctions in water ( $Pr = 6.7$ ), normalized by their respective maxima, for: (a) opposing mixed convection ( $\bar{R} = -\frac{1}{2}$ ), at points  $k$  and  $l$  on figure 11; (b) natural convection ( $\bar{R} = 0$ ), at points  $i$  and  $j$  on figure 10; (c) aiding mixed convection ( $\bar{R} = 1$ ), at points  $g$  and  $h$  on figure 10.

included in that formulation. In air, the location of the velocity profile inflexion point (at  $\eta \approx 1.8$ ) is well inside the thermal boundary layer (see figure 2). However, in water, the inflexion point (at  $\eta \approx 1.4$ ) lies near the outer edge of the thermal layer (see figure 3). This difference in buoyancy force distribution apparently causes large effects.

Some evidence for a secondary unstable region at low  $G$  was also found for aiding mixed convection in water. However, converged eigenvalues and eigenfunctions could not be obtained. Lee *et al.* (1987*b*) did find secondary neutral curves for aiding mixed convection for  $Pr = 7.0$ . The calculations reported here were performed in double precision. These calculations suggest that a secondary neutral curve may exist. However, higher precision is required to resolve this question.

#### 5.4. Opposing mixed convection in water

Figure 11 shows constant- $A$  contours for opposing mixed convection in water ( $\bar{R} = -\frac{1}{2}$ ,  $Pr = 6.7$ ) as dashed lines. Boundary-layer separation does not occur for any values of  $G$  considered in these calculations. The flow is slightly more stable than the corresponding natural-convection flow, both at the location of neutral stability, and further downstream. However, these effects are very small. The most amplified frequency component downstream to  $A = 8$  is  $B = 0.26$ . This is compared to  $B = 0.28$  for natural convection.

Eigenfunctions for water ( $Pr = 6.7$ ) are compared in figure 12. The locations on the stability plane are represented by points ( $g-l$ ) on figures 10 and 11. The temperature disturbance layer is much thinner than the corresponding stream-function disturbance layer. The shapes of the eigenfunctions are once again preserved downstream. However, the maxima occur at  $\eta \approx 1$ , not at the point of inflexion of the undisturbed velocity profile at  $\eta \approx 1.4$ .

## 6. Conclusions

The stability and disturbance-amplification characteristics of a mixed-convection boundary layer adjacent to a vertical, isothermal flat surface have been determined. Linear stability theory and the parallel-flow approximations were used to define an eigenvalue problem which was solved numerically for  $Pr = 0.733$  and 6.7.

Results are given for aiding and opposing mixed convection in air and water, as well as for the corresponding natural-convection flows. For aiding flows in air, an additional region of instability was found, detached from the conventional 'primary' neutral curve. However, disturbance growth in this region was very small. Significant disturbance growth begins downstream of the primary neutral curve. However, this growth is at a slower rate than in natural convection. Downstream disturbance growth is faster for an opposing mixed-convection effect in air. Only a narrow band of disturbance frequency components is amplified downstream, in both aiding and opposing mixed convection. The effect of an aiding forced flow is to increase the frequency level of this band, over the corresponding frequency level for natural convection. Opposing flows caused the opposite effect.

For mixed-convection flows in water, the effect of a free-stream velocity is much smaller than in air. The aiding effect in water is slightly destabilizing. The opposing flows are slightly more stable. As in air, the level of the selectively amplified frequency band increases with an aiding free-stream and decreases with an opposing free stream. Calculations also suggest a secondary detached unstable region in aiding mixed convection in water. However, its existence could not be confirmed.

These results were not compared directly with experiment, since no data are available for the instability of mixed convection adjacent to a vertical isothermal surface. Carey & Gebhart (1983) reported data for aiding mixed convection in air adjacent to a uniform-heat-flux surface. Good agreement with theory was found. The present results are qualitatively similar to those of Carey & Gebhart (1983), except that they did not find a secondary unstable region. Experiments are required to verify this unusual feature. Further experimental results are also needed for opposing mixed convection in gases, and for aiding and opposing mixed convection in liquids.

The authors acknowledge the support through the National Science Foundation grant CBT 84 18517 in this research. They also thank Drs R. Krishnamurthy and Y. Joshi for some very helpful discussions. R. A. B. was supported by the University of Cincinnati during preparation of part of the manuscript.

#### REFERENCES

- AUDUNSON, T. & GEBHART, B. 1976 Secondary mean motions arising in a buoyancy induced flow. *Intl J. Heat Mass Transfer* **19**, 737.
- BREWSTER, R. A. 1988 Experimental studies of natural convection effects on downward freezing of cold pure and saline water, and stability of mixed convection flow adjacent to a vertical isothermal surface. Ph.D. dissertation, University of Pennsylvania, Philadelphia, Pennsylvania.
- CAREY, V. P. & GEBHART, B. 1982 Transport at large downstream distances in mixed convection flow adjacent to a vertical uniform-heat-flux surface. *Intl J. Heat Mass Transfer* **25**, 255.
- CAREY, V. P. & GEBHART, B. 1983 The stability and disturbance amplification characteristics of vertical mixed convection flow. *J. Fluid Mech.* **127**, 185.
- CHEN, T. S. & MOUTSOGLU, A. 1979 Wave instability of mixed convection flow on inclined surfaces. *Numer. Heat Transfer* **2**, 497.
- CHEN, T. S. & MUCOGLU, A. 1979 Wave instability of mixed convection over a horizontal flat plate. *Intl J. Heat Mass Transfer* **22**, 185.
- DRING, R. P. & GEBHART, B. 1968 A theoretical investigation of disturbance amplification in external laminar natural convection flow. *J. Fluid Mech.* **34**, 551.
- ECKERT, E. R. G. & SOEHNGEN, E. 1951 Interferometric studies on the stability and transition to turbulence in a free-convection boundary-layer. *Proc. Gen. Disc. Heat Transfer, ASME and IME, London*, pp. 321.
- ESHGHY, S. 1964 Forced-flow effects on free-convection flow and heat transfer. *Trans. ASME C: J. Heat Transfer* **86**, 290.
- GASTER, M. 1974 On the effects of boundary-layer growth on flow stability. *J. Fluid Mech.* **66**, 465.
- GEBHART, B., JALURIA, Y., MAHAJAN, R. L. & SAMMAKIA, B. 1988 *Buoyancy-Induced Flows and Transport*. Hemisphere.
- HIEBER, C. A. & GEBHART, B. 1971 Stability of natural convection boundary layers: some numerical solutions. *J. Fluid Mech.* **48**, 625.
- JALURIA, Y. & GEBHART, B. 1974 On transition mechanisms in vertical natural convection flow. *J. Fluid Mech.* **66**, 309.
- KNOWLES, C. P. & GEBHART, B. 1968 The stability of the laminar natural convection boundary layer. *J. Fluid Mech.* **34**, 657.
- KRISHNAMURTHY, R. & GEBHART, B. 1989 An experimental study of transition to turbulence in vertical mixed convection flows. *Trans. ASME C: J. Heat Transfer* **111**, 121.
- LEE, S. L., CHEN, T. S. & ARMALY, B. F. 1987a Free stream effects on the wave instability of buoyant flows along an isothermal vertical flat plate. *Intl J. Heat Mass Transfer* **30**, 1556.
- LEE, S. L., CHEN, T. S. & ARMALY, B. F. 1987b Wave instability characteristics for the entire regime of mixed convection flow along vertical flat plates. *Intl J. Heat Mass Transfer* **30**, 1743.

- LEE, S. L., CHEN, T. S. & ARMALY, B. F. 1988 Non-parallel wave instability of mixed convection flow on inclined flat plates. *Intl J. Mass Transfer* **31**, 1385.
- LIN, C. C. 1945 On the stability of two-dimensional parallel flows. Part II – Stability in an inviscid fluid. *Q. Appl. Maths* **3**, 218.
- MERKIN, J. H. 1969 The effect of buoyancy on the boundary-layer flow over a semi-infinite vertical flat plate in a uniform free stream. *J. Fluid Mech.* **35**, 439.
- MUCOGLU, A. & CHEN, T. S. 1978 Wave instability of mixed convection flow along a vertical flat plate. *Numer. Heat Transfer* **1**, 267.
- MUCOGLU, A. & CHEN, T. S. 1979 Mixed convection on inclined surfaces, *Trans. ASME C: J. Heat Transfer* **101**, 422.
- SZEWCZYK, A. A. 1964 Combined forced and free-convection laminar flow. *Trans. ASME C: J. Heat Transfer* **86**, 501.
- WAKITANI, S. 1985 Non-parallel-flow stability of a two-dimensional buoyant plume. *J. Fluid Mech.* **159**, 241.